Article

Roll–to–Roll Manufacturing of Robust Superhydrophobic Coating on Metallic Engineering Materials

shuliang dong, Zhenlong Wang, Yukui Wang, Xuelin Bai, Yong Qing
Richard Fu, Bin Guo, Chaoliang Tan, Jia Zhang, and PingAn Hu

ACS Appl. Mater. Interfaces, **Just Accepted Manuscript** • DOI: 10.1021/acsami.7b16251 • Publication Date (Web): 21 Dec 2017

Roll–to–Roll Manufacturing of Robust Superhydrophobic Coating on Metallic Engineering Materials

Shuliang Dong, [†] *Zhenlong Wang,* [*,†,‡] *Yukui Wang,* [†] *Xuelin Bai,* [†] *Yong Qing Fu,* [§] *Bin Guo,* [*,†] *Chaoliang Tan,* [#] *Jia Zhang,* [*,†,‡] *PingAn Hu* [†]

[†]Key Laboratory of Microsystems and Microstructure Manufacturing, Ministry of Education, Harbin Institute of Technology, No. 2 Yikuang Street, Harbin, 150080, China.

[‡]State Key Laboratory of Robotics and System, Harbin Institute of Technology, No. 2 Yikuang Street, Harbin, 150080, China.

[§]Faculty of Engineering & Environment, Northumbria University, Newcastle upon Tyne, NE1 8ST, UK.

[#]Electrical Engineering & Computer Sciences, University of California at Berkeley, Berkeley, California 94720, United States

KEYWORDS: roll–to–roll manufacturing, robust superhydrophobic surface, EDM, metallic engineering materials, carbon nanoparticles

ABSTRACT: Creating a robust superhydrophobic surface on the conventional engineering materials at mass production is of great importance for self–cleaning, anti–icing, non–wetting surface and low flow resistance in industrial applications. Herein, we report a roll–to–roll

strategy to create durable and robust superhydrophobic surfaces with designed micro–/nano–scale hierarchical structures on many conventional engineering materials by combining electrical discharge machining, coating of carbon nanoparticles, and followed by oil penetration and drying. The treated surface shows good superhydrophobic properties with static water contact angle of 170±2^{o} and slide angle of 3±1^{o}. The treated surface also exhibits good resilience and maintains the performance after tested in various harsh conditions including water flushing for several days, sand abrasion, scratching with sandpapers and corrosive solution. Significantly, the superhydrophobic surfaces also shows a high efficiency of self–cleaning properties even after oil–contamination during applications.

INTRODUCTION

Wettability of a solid surface is critical for both fundamental research and industrial applications. A surface with a water static contact angle (CA) larger than 150° and a sliding angle (SA) smaller than 10° is generally considered as a superhydrophobic surface,[1, 2] which has advantages of non–wetting, self–cleaning and low flow resistance. The lotus surfaces,[3] legs of water striders[4] and butterfly wings[5] are natural examples of superhydrophobicity. Mimicking their surface morphologies using micro–/nano– structures leads to the development of various artificial superhydrophobic surfaces, some of which are being applied in industrial and biological processes.[2, 6] As well known, the water repellent ability of a specific surface is strongly affected by its chemical composition, surface geometric structures (or surface roughness) and superhydrophobicity. Therefore, chemical modifications and development of micro–/nano–scale hierarchical structures are essential to achieve a low surface energy and superhydrophobicity.[2-7] Low surface energy materials were solely employed to modify the rough surface to achieve the superhydrophobicity.[1, 2, 6, 7] However, the weak wear resistance resulted in loss of the water repellency soon.[8] As an alternative, many different surface morphologies have been created to achieve more stable

superhodrophobicity.[2, 6, 8-10] Nevertheless, most of these are limited to polymers and colloidal materials.[11, 12] These types of soft matter surfaces are unlikely to be widely applied in industry owing to their non–scalable–techniques, poor mechanical resistance, and performance degradation with time.[13] Recently, advanced techniques such as laser beam or chemical etching, oxidation, and surface coatings have widely been used, but they often suffer from the using of expensive equipments and/or complicated processes.[14-19] Creating durable and robust superhydrophobic surface for industrial applications, one of the key concerns is how to successfully transfer lab–scale synthesis methods to large–scale and continuous manufacturing processes (such as roll–to–roll), especially for these widely used conventional engineering materials (such as steel, aluminum, copper, metallic composites).

Electrical discharge machining (EDM) is widely used for fast and scalable machining process of metallic engineering materials. The electric discharge (i.e., spark) occurs between the tool electrode and work–piece, transferring the electric energy into a local heating (Figure S1). As a result, an amount of material could be melted and vaporized, leaving large amounts of random distribution of cavities (often called craters) on the work–piece (Figure S1). As the work–piece is moved along the axis (i.e., X axis in Figure 1), the surface will be milled continuously, generating a continuous distribution of craters on the surface. The microscale craters generated on the surface of work–pieces are normally regarded as defects which degrade the machining accuracy,[20-24] but they could be beneficial as a suitable substrate for a superhydrophobic coating. Recently, Chu *et al* achieved the fabrication of hydrophobic surfaces on the stainless steel[20, 21] and aluminum alloy[22] by designing special microscale grooves and then machined using wire EDM. Nevertheless, the machined surfaces exhibited non–uniform wettability with anisotropic properties in the parallel and perpendicular groove directions.[20-22] King *et al* realized a superhydrophobic surface on the steel by fabrication of micro–mushroom re–entrant structures using EDM.[23] Although the complex designs and machining were adopted, these attempts show a non–ideal performance in

superhydrophobicity.[20-23] Meanwhile, they have limited abilities for the large–scale manufacturing with robust surfaces especially on the curved surfaces.

Here, we present a new roll–to–roll strategy to manufacture large–scale, durable and robust superhydrophobic surfaces on many conventional engineering materials. This is realized by combining EDM, coating of carbon nanoparticles, and most importantly, oil penetration and drying. The superhydrophobic properties were evidenced by the static water contact angle of 170±2^{o} and slide angle of 3±1^{o} (Advancing/Receding angle 172±1^{o}/169±2^{o}). The developed superhydrophobic coating surface shows good resilience and maintains its performance after tested in various harsh conditions including water flushing for several days, sand abrasion, scratching with sandpapers and corrosive solution. Our coatings can be used in many areas which are required for self–cleaning applications even after contaminated with oils.

RESULTS AND DISCUSSION

Figure 1 schematically illustrates our strategy for roll–to–roll manufacturing of the superhydrophobic coating on conventional engineering materials. It includes three steps: (I) The work–piece is firstly milled by EDM process to create microscale structures on its surface; (II) The surface is then coated with a layer of carbon nanoparticles by the burning flame of butane to form a superhydrophobic layer; (III) Droplets of penetrating oil is dropped onto the carbon coated surface and then heat–treated, thus transforming the fragile superhydrophobic surface into a durable and robust one.

As mentioned above, EDM process will generate a continuous random distribution of microscale craters on the surface (Figure 1, Figure 2a and Movie S1), which could be used as a platform for superhydrophobic coating. The air was entrapped inside the craters underneath the water droplets, leading to an increase CAs from 66±2° to 95±2° (Figure S2a, b), thus realizing hydrophobicity and water repellency. Thereafter, the superhydrophobic layer was realized by putting the EDM–milled surface facing the outer burning flame of the butane with

a distance of 3–5 cm, and then a layer of carbon nanoparticles (i.e. soots) was deposited on the milled surface as illustrated in Figure 1, Figure 2e and Movie S1. It can be seen that the color of the sample surface was changed from luminous yellow (e.g. EDM milled copper surface) to dark black (see Movie S1).[25, 26] After the flame deposition, the CA values were found to increase from 95±2° to 168±2° (Figure S2b, c), indicating the formation of a superhydrophobic coating on the surface of work–piece. However, these carbon nanoparticles have been proved very fragile since the interactions among carbon nanoparticles are only physical ones and relatively weak.[25, 26] When the water drop rolled off on the surface, it carried away some of the soot (Movie S2) and the drop underwent a wetting transition from 168±2° to 136±5°. Obviously, it was impossible for the surfaces to withstand the harsh conditions such as flushing of water and provide a long–term and high performance of water–repellency. In order to improve the stability of the surface, the penetrating oils such as kerosene were sprayed onto the coated carbon layer, and then heat–treated at 310 ^{o}C for 3–5 minutes. The durability of the superhydrophobic coating was found to be improved significantly and the CA can be further increased to 170±2° (Figure S2d). The values of advancing and receding contact angle are summarized in Table S1.

As mentioned above, the superhydrophobic surface could be achieved by both modifying surface structures and decreasing the surface energy. We systematically investigated the morphology of each step to evaluate the hierarchical structures of coating. Figure 2b shows a typical scanning electron microscope (SEM) image of EDM milled copper surface with randomly distributed craters. An enlarged SEM image (Figure 2c) shows a smooth surface within craters and a few nanoscale clusters deposited at the bottom of the craters (Figure 2d). The average lateral diameter and depth of craters are in the range of 10–20 μm and 1.3–2.5 μm, respectively, at an EDM discharge current of 1.75 A, leading to an average roughness of 1.36 μm (value of R_a, see Figures S3 and S4). The structural size of craters can be facilely controlled by varying the discharge current at a given voltage (Figures S3 and S4). Therefore,

the surface roughness can be controlled to achieve the optimal superhydrophobic condition (Figure S5).

The burning flame of butane provides a layer of carbon soots to the sample surfaces with, which in principle does not change morphology of EDM milled surfaces at microscale (Figure 2f), but will partially fill the inner spaces of craters with numerous carbon nanoparticles (Figure 2g,h). Herein, a strong synergistic effect of hierarchical structures from microscale craters and nanoscale carbon soots leads to an improved superhydrophobility with CA values of 168±2° and SA values of 4±1° (Advancing/Receding angle 170±1°/166±2°), respectively (Figure S2c). The penetration and drying processes of penetrating oil (kerosene used in this study shown in Figure 2i) create more nanoscale convex structures on carbon soots (Figure 2k, l) during the shrinking and drying of kerosene without noticeably influencing the microscale craters (Figure 2k, l). The water–repellency has also been improved and the obtained average CA values are 170±2° and SA values of 3±1° (Advancing/Receding angle 172±1° /169±2°) (Figure S2d, Figure S5, and Movie S3). The randomly distributed carbon nanoparticles are clustered together under the driving force of the capillary force, which is generated during the evaporation and drying stage of the kerosene.

To identify the functionality of the craters, a smooth surface of C17200 was machined by using the conventional turning and milling, respectively. Both of surfaces show a smaller roughness (Ra 0.8) compared with the EDM milled surface (Ra 1.36, Figure S6). After the same flame deposition and kerosene penetration and drying process, the CAs and SAs on the turning surfaces are only 150±2° and 7±3° (Figure S6d inset), while they are 147±2° and 10±4° on the milling surface (Figure S6g inset), respectively. Obviously, both of smooth surfaces exhibit a worse superhydrophobicity. Therefore, the rough surface with a microscale structures is better in this case as the platform for superhydrophobic coating.

In order to verify the chemistry changes on the sample surfaces, we have investigated the crystalline structures and chemical states on the sample surfaces after each key process. X–ray

diffraction (XRD) pattern (Figure 3a) shows that there are two broad and weak peaks around $2\theta=24.3^{o}$ and 43.2^{o} corresponding to the (002) and (100) planes of typical turbostratic graphite, indicating that the disordered carbon structures were formed during the EDM milling (Figure 3a black curve). These structures were reported to appear in the EDM process by using the kerosene as electrolyte.[27] After the flame deposition of soot and penetration and drying of kerosene, the two diffraction peaks became sharpened with increased intensity revealing the formation of graphite crystals (Figure 3a blue and red curve). The newly observed diffraction peak at 17.9° could be assigned to C60 formed during drying of kerosene in air, which is consistent with those reported in literatures.[28-30] No other new diffraction peaks were observed, indicating that there was no new chemical compound formed during the later process. Furthermore, transmission electron microscope (TEM) image of flame deposited soot shows agglomerated particles which are spherical with diameters in the range of 20–50 nm (Figure S7a). High resolution TEM image displays the solid spherical morphologies with turbostratic structure in atomic lattice (Figure S7b), which is consistent with the XRD results shown in Figure 3a. After kerosene penetration and drying, the interplanar spacing is the same as before (Figure S7c, d). It is about 0.365 nm for both samples (Figure S7b, d), which is similar to the XRD results in Figure 3a. Raman spectra (Figure 3b) shows only two clear peaks centered at ~1340 cm^{-1} (D peak) and ~1580 cm^{-1}(G peak) in all the steps, which are assigned to turbostratic graphite characters of coating.[29] No apparent peak shift indicates that there are no changes in the vibration modes and chemical bonds or coating stress. High–resolution XPS C1s spectra (Figure 3c) reveal typical carbon structures hybridized with planar hexagonal graphitic rings of sp^2 (normalized at 284.5 eV) and tetrahedral structure of sp^3 (285.6±0.3 eV).[31] The other peaks at 288.8±1.1 eV (Figure 3c blue curve) and 286.4 eV (Figure 3c red curve) are assigned to C=O and C–O, respectively, which are mainly from oxidation of carbon during flame based soot deposition and kerosene drying process, as well as surface adsorption. It is noteworthy to point out that the absence of

carbon–copper bond indicates that only physical adsorption of carbon happens on the surface. All the spectra in Figure 3 reveal that only a layer of carbon coating on the treated surface without other apparent carbon based chemical bonds detected. Therefore, the impressive superhydrophobicity and water repellency can be solely attributed to the formation of micro–/nano– structures.

To highlight advantages of our method, we have compared the CA values of our achievements with the related results reported in the literatures (Figure S8).[20-23, 25, 26, 32-34] The CA values of carbon coatings on smooth surfaces (i.e., silicon wafer and glass slide) were found to be in the range of 145–160^{o}, whereas they were found to be 154–162^{o} on the EDM milled surface without further treatment. Obviously, the synergistic effect of micro craters and carbon nanoparticles in our method promotes the water–repellency ability to its maximum, showing the merits of our strategy.

Since the EDM is a powerful technology to control the morphology of milled surface, the superhydrophobic features can be facilely modified (Figures S3-S5). For instance, applying a higher discharge current in the EDM process provides much higher energy in one pulse, leading to much more materials to be removed in the unit time. Thus, larger sizes of craters with higher roughness can be achieved on the samples discharged (Figures S3 and S4). In addition, since the EDM method has a capacity of machining all types of metallic materials, we have successfully obtained superhydrophobic coatings on various conventional engineering materials as shown in Figure 1 bottom left. Therefore, based on the integration of industry–scale processes of EDM technology, flame deposition and penetration and drying of oil, we have developed a facile and scalable roll–to–roll compatible approach to create superhydrophobic coating on conventional engineering materials.

The poor surface robustness is the main issue limiting the widespread industrial applications of most currently developed superhydrophobic coatings, since the commonly used chemical modification and nanoscale structures are frequently mechanically weak and

readily abraded/damaged.[35] Our newly designed superhydrophobic surface shows good resilience and maintains its performance after various harsh tests including several days of water flushing, sand abrasion and sandpapers scratching (Figure S9). For example, impingement the coating surfaces using water droplets with a diameter of 2.6±0.3 mm and a velocity of 1.4 m s^{-1} (the velocity is equal to those in a vernal rain) did not cause apparent damage of the water–repellency ability for at least 7 days, whereas the superhydrophobic surface lasted at least 3 days with a good performance when the impingement velocity was increased to 2 m s^{-1} (Figure S9a and Movie S4). This shows a significantly improved durability compared with those reported in the literature using the carbon nanoparticles coated with SiO_2 substrates[36] or sprayed TiO_2 nanoparticles[37] as well as carbon soot coated on smooth plate.[32, 33, 38, 39]

Sand impinging was also used to test the mechanical durability of our developed superhydrophobic surfaces, using the sand particles with an average diameter of 300–500 μm and an impinging velocity of 2.5–3.0 m s^{-1} corresponding to an impinging energy of 1.4~6.9×10^{-7} J (Figure S9b). This similar impinging condition was used in ref. 26 which was reported to heavily damage the superhydrophobic surface.[26] Nevertheless, our newly developed coating still rendered a good water–repellency properties and the superhydrophobic coating still showed a high CA of 160° after 40 g sands impinging at the same position (Figure S9c). Another 10–20 g sands were needed to damage the superhydrophobicity of the beneath coating at the same position, which led to the significant decreases of the CA below 150°.

We also performed sandpaper abrasion tests with coated surface faced–down to sandpaper (Grit No. 1000) under a normal weight of 50 g (i.e., estimated normal pressure of 1.357 kPa) and then moved the coated surfaces on the sandpaper with a reciprocating speed of 18–25 mm s^{-1} (Figure S9d). The CA values were measured after each 100 mm long abrasion distance and the results are summarized in Figure 4a. The CA values were kept in the range of 150°–172°

with a 1200 mm long abrasion, indicating a robust superhydrophobic coating without significant damages under the tested mechanical abrasion. Meanwhile, the SA values were measured to be below ~10° within 300 mm abrasion distance, but the values were found to increase with the increase of the abrasion distance (Figure 4a). Obviously, there are two stages of hydrophobic modes within the 1200 mm sandpaper abrasion distance, which would be discussed in future. Furthermore, a scotch tap test was proceed to evaluate the adhesion performance of the as–prepared superhydrophobic coatings.[40, 41] Figure S10 shows a gradually decrease of CA value from 172° to 155° within six peeling attempts on the oil penetration and drying coatings, while it rapidly decreases at the second peeling attempt on the flame deposition soot. As a result, as–prepared superhydrophobic coating has a relative strong adherence between the substrate and coating.

To reveal the corrosive properties of as-prepared superhydrophobic coatings, they were investigated by the potentiodynamic polarization curves (Tafel) and electrochemical impedance spectroscopy (EIS) in the 3.5 wt% NaCl solution at room temperature. Figure 4b shows the Tefel curves of the C17200 surface at each state during the superhydrophobic coating. The values of corrosion potential (E_{corr}) and corrosion current density (i_{corr}) were obtained by Tafel extrapolation from the potentiodynamic polarization curves.[42, 43] The details of Tafel polarisation curves are summarized in Table S2. Therefore, the inhibition efficiency (η_{IE}) corresponding to the corrosion resistance property can be calculated by,[44, 45]

$$\eta_{IE} = \frac{i_0 - i_{corr}}{i_0} \times 100\% \quad (1)$$

Where i_0 and i_{corr} are the current density collected from the original C17200 surface and as-prepared superhydrophobic surface, respectively. The E_{corr} of the surface after penetration and drying process can reach 28 mV, which is quite more positive than the original surface (-81 mV), EDM milled surface (-83 mV) and Flame deposition soot surface(-27 mV). The i_{corr} of the surface lows to 6.31×10^{-8} A cm^{-2} which is decreased by more than 4 order magnificent

compared to that of the original surface (3.47×10^{-4} A cm^{-2}). Meanwhile, as-prepared superhydrophobic surface shows the largest η, about 10 times compared to EDM milled surface, indicating an achievement of good anticorrosion protection with coating.

Furthermore, EIS tests were carried out to evaluate the electrochemical corrosion behaviors and anticorrosion of as-prepared superhydrophobic coatings. Figure 4c and d shows the Nyquist plots and Bode plots of the C17200 sample at each process. The diameter of the impedance semicircle represents the polarization resistance of the work electrode (i.e., C17200 sample at each stage). Significantly, it increases sharply approaching to a hundred of $k\Omega\cdot cm^2$ after oil penetration and drying process (Figure 4c), which is about 400 times compared to the original and after EDM milled material. Figure 4d shows the Bode plots (impedance modulus |Z| as a function of frequency) of the four samples in 3.5 wt % NaCl solution. As-prepared superhydrophobic surface has the highest impedance value around 150 $k\Omega\cdot cm^2$, which is 2 orders of magnitude larger than that of original surface or EDM milled, and 1 orders of magnitude larger than that of flame deposition soot in the low frequency region. According to EIS tests, as-prepared superhydrophobic coating provides excellent corrosion protection for bare C17200 substrate.

To reveal the potential application in the highly saline environment,[46] we have compared the long-term stability of superhydrophobic surface before and after penetration and drying process in the 3.5 wt% NaCl solution. After penetration and drying process, the superhydrophobic coating exhibits a promising stability up to 39 hours, while it merely lasts ~3 hours without further process (Figure S11a). The loose carbon soots and low adhesion to substrate after the flame deposition was easily damaged by the corrosive solution, resulting in decreasing ability of water repellency. Further oil penetration and drying process will dense the carbon soots and improve the adhesion to the substrate, leading to an enhancement of stability up to 39 hours. Figure S11b shows a digital picture of two piece of C17200 samples immersing in corrosive solution. The bright surface after 3 hours corrosion suggests the air

can be still trapped on the substrate and form the air film between the as–prepared superhydrophobic surface and solution.[41] The EDM milled surface only with flame deposition became dark green after 39 hours corrosion (Figure S11c), indicating a heavy peeling off carbon soot from the substrate, while the oil-treated surface was keeping bright color.

The coated surface shows good self–cleaning properties from the bouncing–water and continuous flushing droplets. Herein, cupric chloride hydrate ($CuCl_2 \cdot 2H_2O$) powder as the artificial dirt was deliberately spread onto the coated surface (Figure 5a), and then collected and carried away by the rolling off droplet and left a cleaning line along its flow trajectory (Figure 5b). The final color of the rolling droplet becomes light green, indicating the effective removal of dirt. This change can be explained by the droplet's picking up the dirt during its rolling on the surface (Figure 5e). Usually, the superhydrophobic coatings are very fragile to oil contamination, losing their self–cleaning properties.[47] However, our superhydrophobic surface has already been pretreated with oil during preparation (Figure 1, step III), and further oil contaminants during service would not degrade its self–cleaning ability. Figure 5c,d show the rolling off of water droplets on the oil contaminated coatings, and the dirt was removed along the trajectory although the droplet was not a perfect sphere due to wettability of oil contaminants (Figure 5d). The principle can be explained using Figure 5f, which is similar to those for the slippery liquid infused porous surfaces.[48, 49]

The mechanism of enhanced water repellency can be explained by the thermodynamic formula.[50] Figure S12a and b show a typical SEM image of the EDM milled C17200 surface after the flame deposition and oil penetration and drying process, respectively. Many protrusions were formed between the adjacent craters after EDM milled. Figure S12c shows a model of cross section of the protrusions shown in Figure S12a, in which the outline of protrusion is smaller than a semicircle ($\alpha<\pi/2$). According to Ref. 50, the water droplets tends to be a homogeneous wetting as $\alpha<\pi/2$. Therefore, the contact angle can be expressed as:

$$\cos\theta = \begin{cases} r\cos\theta_p & r\cos\theta_p \geq -1 \\ -1 & otherwise \end{cases} \quad (2)$$

where r and θ_p represents the roughness ratio and represents the contact angle of carbon particles deposited on a plane, respectively. After oil penetration and drying process, the thickness of carbon soot reduced to ~1/4 of its original thickness (Figure 6d, e), leading to the outline of protrusion bigger than a semicircle ($\alpha>\pi/2$) shown in Figure S12d. In this condition, the contact angle can be expressed as

$$\cos\theta = \left(\pi - \theta_p\right)\cos\theta_p + \sin\theta_p - 1 \quad (3)$$

Since the θ_p was in the range of 145–160°,[25,26,32-34] the CAs were calculated to be in the 157.9-170.4° by Eq (3). In our experiments, the CAs of as-prepared superhydrophobic coatings were 170±2°, which are consistent with the theoretical values (157.9-170.4°).

The enhancement of durability of superhydrophobic coating could be explained by improved adhesion among carbon nanoparticles and improved adhesion to the substrate by the clustering of carbon nanoparticles during the penetration and drying processes. Figure 6a-c illustrate the mechanism induced by the morphology change of carbon nanoparticles. The porous structure (Figure 6a, d, g) and intrinsic oil wetting properties of deposited carbon soots make the kerosene fully penetrating into the carbon layer (Figure 6a). At the drying stage, carbon nanoparticles are subjected to capillary forces at the liquid–gas–solid interfaces (Figure 6b). The capillary pressure (Δp) between two sphere particles on the liquid–solid interface is given by Laplace's formula:[51]

$$\Delta p = \gamma\left(\frac{1}{R_1} - \frac{1}{R_2}\right) \quad (4)$$

where R_1 and R_2 are the principal radii of the external curvature of the bridge surface, and γ is the surface tension between the kerosene–air interface.

For a cylindrical capillary of radius R and liquid on a substrate with a wetting angle θ, the pressure, Δp, can be rewritten by:

$$\Delta p = \frac{2\gamma \cos\theta}{R} \quad (5)$$

As the wetting liquid (e.g. kerosene) occupies a position with the highest capillary potential, it carries the carbon nanoparticles to coalescence together spontaneously thereby forming capillary pores (Figure 6b). During the drying process, the moving kerosene tends to occupy those positions who can ensure the minimum energy of whole system. Therefore, a lot of meniscuses are formed among the carbon nanoparticles, pulling or pushing apart the neighbouring particles (Figure 6b). The magnitude of capillary forces depends on the size of meniscus (R) and different amplitudes of stresses are generated which cause the cluster of particles as shown in Figure 6f. Obviously, there is a continuous increase of capillary pressure during the evaporation of kerosene (Figure 6f), which makes the soot layer become denser (Figure 6c, h). The clustered of carbon nanoparticles will significantly reduce the thickness of carbon soot (e.g. from 17 μm to 4 μm, Figure 6d, e), densify the soot layer, and improve its adhesion to the substrate (Movie S5). Enlarged cross–section SEM images of carbon nanoparticles in Figure 6d, e show the dense film after dried. As a result, the elastic modulus of the carbon layer was increased from 0.387 GPa to 0.916 GPa measured from nanoindentation before and after kerosene penetration and drying process (Figure 6i). In addition, the protrusion between the adjacent craters will protect the carbon nanoparticles within them from carrying out by the drop water or mechanical abrasion (Figure S13). The carbon nanoparticles in the protrusion areas (Figure S13, marked with red circles, area A) were removed by the scratching or impinging, while they kept the same within the craters (Figure S13 marked with yellow circles, area B). Thus, the superhydrophobicity did not change dramatically as the abrasion going on. The densification of carbon nanoparticles and increased elastic modulus will enhance the resistance of external mechanical damage such as

water flushing, sand abrasion and scratching thereby enhancing the stability of superhydrophobic coatings.[52, 53]

CONCLUSION

We presented a roll–to–roll manufacturing strategy for durable and robust superhydrophobic surfaces on conventional engineering materials by combining EDM, carbon nanoparticle deposition and oil penetration and drying process. The controlled microscale craters on EDM surface provide an ideal platform for deposition of carbon nanoparticles to form a hierarchical micro–/nano– structures, which showed quite good water–repellency and superhydrophobicity with an CA up to 170±2° and SA values of 3±1°(Advancing/Receding angle 172±1°/169±2°). The oil penetration and drying process densified the carbon layer and increases the strength by ~3 times, thereby providing the good durability under the harsh water flushing, mechanical abrasion and corrosion testing. Furthermore, the superhydrophobic coatings also showed a high efficiency of self–cleaning properties even after oil–contamination during applications.

EXPERIMENTAL SECTION

Roll–to–roll superhydrophobic coating of engineering materials. In the experiments, foils/plates of various engineering materials (typical thickness of 50 μm), including beryllium copper alloy (C17200), titanium alloy (Ti–6Al–4V), stainless steel (06Cr19Ni10), aluminum alloy (Al2024), Ni–based superalloy (GH4169), were purchased from DongGuan Jia Sheng Copper Co., Ltd, China, and then ultrasonically cleaned in ethanol and deionized water before used in the EDM machining. A bulk of copper (99.9% purity) with length of 10 mm and width of 25 mm was used as the tool electrode. The foil was programmed to move by a feed roller and generated a machined track at a speed of 0.24–0.5 mm s^{-1} (Figure 1 and Movie S1). The typical materials removal rate was about 18–31 mm^3 min^{-1}. During the process, an EDM milling was firstly carried out with a commercial EDM machine,[54] and the tool electrode (cathode) and a work–piece (anode) were immersed in the kerosene (dielectric work solution, EDM–3, Mobil, SUA). After ultrasonically cleaning, the milled surface was faced vertically

to the flame of butane with a distance of 3–5 mm from outside flame. With a butane consuming rate of 1.5 sccm (standard–state cubic centimeter per minute), a black carbon layer has been deposited onto the milled metal surfaces. Finally, the penetrating oil such as kerosene was dropped onto the carbon layer at a rate of about 1–5 μL s^{-1} and then heated to 310 ^{o}C in air for 3–5 min to evaporate the kerosene (Figure 1 and Movie S1).

Characterization. The surface treated foils were cut into pieces with dimensions of 12×25 mm^2 for the characterization. The morphology of the specimens was analyzed using a scanning electron microscope (SEM, Supra 55 Sapphire, Carl Zeiss, Germany) at an acceleration voltage of 10 kV and a transmission electron microscopy (TEM, JEM–2100F, JEOL, Japan) at an acceleration voltage of 200 kV. The 3D morphology and corresponding profile curves were characterized using a laser confocal microscope (OLS3000, Olympus, Japan). XRD patterns of the samples were analyzed using X–ray diffractometer (XRD, Empyrean, Panalytical, Netherlands) with Cu Kα1 λ=0.154 nm. Chemical states of elements were analyzed using X–ray photoelectron spectroscopy (XPS, ESCALAB 250XI, Thermo Fisher Scientific, USA). Raman spectroscopy (LabRAM XploRA, incident power of ~1 mW, pumping wavelength of 532 nm) was used to obtain the lattice vibration and chemical bonding information. Elastic moduli of as–coated and oil treated carbon layers on substrate were measured using nanoindentation (Nano–indenter G200, Agilent, USA). The indentation force–displacement curves were analyzed by a method outlined by Domke to calculate each elastic modulus.[55] Water static contact angle (CA), and sliding angle (SA) were measured using an optical contact angle meter system (JC2000C1, Shanghai Zhongchen Digital Technic Apparatus Co., Ltd. China) in air at room temperature. A droplet of 5 μL water was used in each test and five different readings at different areas on the surface of specimens were measured to obtain an average value. The static contact angle was calculated using the Young–Laplace method.[56, 57] In this paper, CA and SA refer to water static contact angle and water sliding angle in the paper respectively, unless specifically noted.

Mechanical and corrosion durability tests of superhydrophobic coatings. The durability of the as–prepared superhydrophobic surface resistance to impinging of water drops was tested with the water drops fall down to the coating from 100 mm (velocity of 1.4 m s^{-1}) and 210 mm (velocity of 2 m s^{-1}) height. The substrate was fixed with a titling angle of 45° to ground (Figure S9a). The diameter of the water drops was about 2.6±0.3 mm. The time interval between two water drops was about 0.5–0.8 s. In addition, sandpaper abrasion and sand impinging tests were employed to evaluate the mechanical durability. The coated surface was faced down to sandpaper (Grit No. 1000) with a normal weight of 50 g (i.e., estimated normal pressure of 1.357 kPa) and moved at a reciprocating speed of 18–25 mm s^{-1} (Figure S9d). The CA values were measured after each 100 mm long abrasion. The sand impinging test was performed using the sand grains with diameter of 300–500 μm and an impinging velocity of 2.5–3.0 m s^{-1} corresponding to an impinging energy of 1.4~6.9×10^{-7} J. The substrate was fixed with a tilting angle of 45° to ground (Figure S9b). According to the ASTM D3359-02 standard, the Scotch tape test was carried out to evaluate the adhesion performance of as-prepared superhydrophobic coating. In detail, a piece of tape was firstly pressed against the as-prepared superhydrophobic coating. And then, the contact angle was measured after each peeling attempt. Each of the reported CA represents the average of five measurements at different positions. Electrochemical corrosion behavior was examined by potentiodynamic polarization curves (Tafel) and electrochemical impedance spectroscopy (EIS) in 3.5 wt% NaCl solution at room temperature on the electrochemical workstation (CHI660D, CH Instruments Inc.). The experiments were performed in a three-electrode cell with a graphite electrode as the counter electrode, as-prepared sample as the working electrode, and silver/silver chloride (Ag/AgCl, 3 M KCl) electrode as the reference electrode. Polarisation curves were recorded at a scanning rate of 1 mV·s^{-1}. EIS experiments were carried out at frequencies ranging from 10^5 to 10^{-2} Hz at open circuit potential with the amplitude of the perturbation voltage of 10 mV. The as-prepared superhydrophobic surface was immersed in

3.5 wt% NaCl solution for a long time to reveal the potential application in the highly saline environment. Each test was repeated more than three times to verify the repeatability of the results.

ASSOCIATED CONTENT

Supporting Information

Supporting information contains: EDM scheme, characteristics, additional graphs, tables and images (Figures S1−S13)

Tables (Table S1 and S2)

Video S1-S5 (AVI)

AUTHOR INFORMATION

Corresponding Author

*wangzl@hit.edu.cn. *guobin@hit.edu.cn. *zhangjia@hit.edu.cn

Author Contributions

J. Z and Z. L. W supervised the project with designing the experiment and analyzing the results. S. L. D carried out the experiments, characterization, testing. and wrote the draft. X. L. B and Y. K. W performed some tests. Y. Q. F, P. A. H , B. G and C.T. provided modifications on the draft. All the authors discussed the results and commented on the manuscript.

Notes

The authors declare no competing financial interest.

ACKNOWLEDGMENT

This project is supported by National Natural Science Foundation of China (Grant No. 51775145, 61771156), Application of Technology Research and Development Program of Heilongjiang province (Grant No. GA16A404). Project supported by the Foundation for Innovative Research Groups of the National Natural Science Foundation of China (Grant

No.51521003), Project supported by the Foundation for Innovative Research Groups of the National Natural Science Foundation of China (Grant No.51521003).

REFERENCES

1. Nakajima, A.; Fujishima, A.; Hashimoto, K.; Watanabe, T. Preparation of Transparent Superhydrophobic Boehmite and Silica Films by Sublimation of Aluminum Acetylacetonate. *Adv. Mater.* **1999**, *11*, 1365-1368.

2. Sun, T.; Feng, L.; Gao, X.; Jiang, L. Bioinspired Surfaces with Special Wettability. *Acc. Chem. Res.* **2005**, *38*, 644-652.

3. Barthlott, W.; Neinhuis, C. Purity of the Sacred Lotus, or Escape from Contamination in Biological Surfaces. *Planta* **1997**, *202*, 1-8.

4. Gao, X.; Jiang, L. Biophysics: Water-Repellent Legs of Water Striders. *Nature* **2004**, *432*, 36-36.

5. Zheng, Y.; Gao, X.; Jiang, L. Directional Adhesion of Superhydrophobic Butterfly Wings. *Soft Matter* **2007**, *3*, 178-182.

6. Zhang, P.; Lv, F. Y. A Review of the Recent Advances in Superhydrophobic Surfaces and the Emerging Energy-Related Applications. *Energy* **2015**, *82*, 1068-1087.

7. Ma, M.; Hill, R. M.; Rutledge, G. C. A Review of Recent Results on Superhydrophobic Materials Based on Micro- and Nanofibers. *J. Adhes. Sci. Technol.* **2008**, *22*, 1799-1817.

8. Hoshian, S.; Jokinen, V.; Somerkivi, V.; Lokanathan, A. R.; Franssila, S. Robust Superhydrophobic Silicon without a Low Surface-Energy Hydrophobic Coating. *ACS Appl. Mater. Interfaces* **2015**, *7*, 941-949.

9. Wang, J.; Liu, F.; Chen, H.; Chen, D. Superhydrophobic Behavior Achieved from Hydrophilic Surfaces. *Appl. Phys. Lett.* **2009**, *95*, 084104.

10. Liu, T. L.; Kim, C. J. Turning a Surface Superrepellent Even to Completely Wetting Liquids. *Science* **2014**, *346*, 1096-1100.

11. Jung, Y. C.; Bhushan, B. Contact Angle, Adhesion and Friction Properties of Micro- and Nanopatterned Polymers for Superhydrophobicity. *Nanotechnology* **2006**, *17*, 4970-4980.

12. Chiou, N. R.; Lu, C.; Guan, J.; Lee, L. J.; Epstein, A. J. Growth and Alignment of Polyaniline Nanofibres with Superhydrophobic, Superhydrophilic and Other Properties. *Nat. Nanotechnol.* **2007**, *2*, 354-357.

13. Morra, M.; Occhiello, E.; Marola, R.; Garbassi, F.; Humphrey, P.; Johnson, D. On the Aging of Oxygen Plasma-Treated Polydimethylsiloxane Surfaces. *J. Colloid Interface Sci.* **1990**, *137*, 11-24.

14. Dong, C.; Gu, Y.; Zhong, M.; Li, L.; Sezer, K.; Ma, M.; Liu, W. Fabrication of Superhydrophobic Cu Surfaces with Tunable Regular Micro and Random Nano-Scale Structures by Hybrid Laser Texture and Chemical Etching. *J. Mater. Process. Technol.* **2011**, *211*, 1234-1240.

15. Kietzig, A. M.; Hatzikiriakos, S. G.; Englezos, P. Patterned Superhydrophobic Metallic Surfaces. *Langmuir* **2009**, *25*, 4821-4827.

16. Wang, S.; Feng, L.; Jiang, L. One-Step Solution-Immersion Process for the Fabrication of Stable Bionic Superhydrophobic Surfaces. *Adv. Mater.* **2006**, *18*, 767-770.

17. Xie, Q.; Fan, G.; Zhao, N.; Guo, X.; Xu, J.; Dong, J.; Zhang, L.; Zhang, Y. Facile Creation of a Bionic Super-Hydrophobic Block Copolymer Surface. *Adv. Mater.* **2004**, *16*, 1830-1833.

18. La, D. D.; Nguyen, T. A.; Lee, S.; Kim, J. W.; Kim, Y. S. A Stable Superhydrophobic and Superoleophilic Cu Mesh Based on Copper Hydroxide Nanoneedle Arrays. *Appl. Surf. Sci.* **2011**, *257*, 5705-5710.

19. Yang, J.; Zhang, Z.; Men, X.; Xu, X.; Zhu, X. A Simple Approach to Fabricate Regenerable Superhydrophobic Coatings. *Colloids Surf., A* **2010**, *367*, 60-64.

20. Bae, W. G.; Kim, D.; Song, K. Y.; Jeong, H. E.; Chu, C. N. Engineering Stainless Steel Surface Via Wire Electrical Discharge Machining for Controlling the Wettability. *Surf. Coat. Technol.* **2015**, *275*, 316-323.

21. Wan, Y.; Lian, Z.; Xu, J.; Weng, Z.; Yin, X.; Yu, H. Fabrication of the Stainless Steel Surface with Super Durable One-Direction Superhydrophobicity and Two-Direction Anisotropic Wettability. *Micro Nano Lett.* **2014**, *9*, 712-716.

22. Bae, W. G.; Song, K. Y.; Rahmawan, Y.; Chu, C. N.; Kim, D.; Chung do, K.; Suh, K. Y. One-Step Process for Superhydrophobic Metallic Surfaces by Wire Electrical Discharge Machining. *ACS Appl. Mater. Interfaces* **2012**, *4*, 3685-3691.

23. Patricia, B. W.; Eduardo, J. T.; Mark, R.; Anthony, M. J.; William, P. K. Hydrophobic and Oleophobic Re-Entrant Steel Microstructures Fabricated Using Micro Electrical Discharge Machining. *J. Micromech. Microeng.* **2014**, *24*, 095020.

24. Chen, S.; Lin, M.; Huang, G.; Wang, C. Research of the Recast Layer on Implant Surface Modified by Micro-Current Electrical Discharge Machining Using Deionized Water Mixed with Titanium Powder as Dielectric Solvent. *Appl. Surf. Sci.* **2014**, *311*, 47-53.

25. Naha, S.; Sen, S.; Puri, I. K. Flame Synthesis of Superhydrophobic Amorphous Carbon Surfaces. *Carbon* **2007**, *45*, 1702-1706.

26. Deng, X.; Mammen, L.; Butt, H. J.; Vollmer, D. Candle Soot as a Template for a Transparent Robust Superamphiphobic Coating. *Science* **2012**, *335*, 67-70.

27. Mohri, N.; Fukuzawa, Y.; Tani, T.; Sata, T. Some Considerations to Machining Characteristics of Insulating Ceramics-Towards Practical Use in Industry. *CIRP Ann-Manuf. Technol.* **2002**, *51*, 161-164.

28. Zhang, W.; Gong, X.; Liu, C.; Piao, Y.; Sun, Y.; Diao, G. Water-Soluble Inclusion Complex of Fullerene with γ-Cyclodextrin Polymer for Photodynamic Therapy. *J. Mat. Chem. B* **2014**, *2*, 5107-5115.

29. Rajan, A. S.; Sampath, S.; Shukla, A. K. An *in Situ* Carbon-Grafted Alkaline Iron Electrode for Iron-Based Accumulators. *Energy Environ. Sci.* **2014**, *7*, 1110-1116.

30. Zhu, H.; Li, X.; Han, F.; Dong, Z.; Yuan, G.; Ma, G.; Westwood, A.; He, K. The Effect of Pitch-Based Carbon Fiber Microstructure and Composition on the Formation and Growth of Sic Whiske/rs Via Reaction of Such Fibers with Silicon Sources. *Carbon* **2016**, *99*, 174-185.

31. Peng, C.; Lang, J.; Xu, S.; Wang, X. Oxygen-Enriched Activated Carbons from Pomelo Peel in High Energy Density Supercapacitors. *RSC Adv.* **2014**, *4*, 54662-54667.

32. Zhou, Y.; Wang, B.; Song, X.; Li, E.; Li, G.; Zhao, S.; Yan, H. Control over the Wettability of Amorphous Carbon Films in a Large Range from Hydrophilicity to Super-Hydrophobicity. *Appl. Surf. Sci.* **2006**, *253*, 2690-2694.

33. Banerjee, D.; Mukherjee, S.; Chattopadhyay, K. K. Controlling the Surface Topology and Hence the Hydrophobicity of Amorphous Carbon Thin Films. *Carbon* **2010**, *48*, 1025-1031.

34. Tian, H.; Wang, F.; Ge, S.; Ou, J.; Li, W.; Yu, S. A Simple and Effective Way to Fabricate Mechanical Robust Superhydrophobic Surfaces. *RSC Adv.* **2016**, *6*, 28563-28569.

35. Lu, Y.; Sathasivam, S.; Song, J.; Crick, C. R.; Carmalt, C. J.; Parkin, I. P. Robust Self-Cleaning Surfaces That Function When Exposed to Either Air or Oil. *Science* **2015**, *347*, 1132-1135.

36. Hsieh, C. T.; Wu, F. L.; Yang, S. Y. Superhydrophobicity from Composite Nano/Microstructures: Carbon Fabrics Coated with Silica Nanoparticles. *Surf. Coat. Technol.* **2008**, *202*, 6103-6108.

37. Teisala, H.; Tuominen, M.; Aromaa, M.; Mäkelä, J. M.; Stepien, M.; Saarinen, J. J.; Toivakka, M.; Kuusipalo, J. Development of Superhydrophobic Coating on Paperboard Surface Using the Liquid Flame Spray. *Surf. Coat. Technol.* **2010**, *205*, 436-445.

38. Schulz, H.; Leonhardt, M.; Scheibe, H. J.; Schultrich, B. Ultra Hydrophobic Wetting Behaviour of Amorphous Carbon Films. *Surf. Coat. Technol.* **2005**, *200*, 1123-1126.

39. Zhou, Y.; Wang, B.; Zhang, X.; Zhao, M.; Li, E.; Yan, H. The Modifications of the Surface Wettability of Amorphous Carbon Films. *Colloids Surf., A* **2009**, *335*, 128-132.

40. Barthwal, S.; Kim, Y. S.; Lim, S. H. Mechanically Robust Superamphiphobic Aluminum Surface with Nanopore-Embedded Microtexture. *Langmuir* **2013**, *29*, 11966-11974.

41. Lu, Z.; Wang, P.; Zhang, D. Super-Hydrophobic Film Fabricated on Aluminium Surface as a Barrier to Atmospheric Corrosion in a Marine Environment. *Corros. Sci.* **2015**, *91*, 287-296.

42. She, Z.; Li, Q.; Wang, Z.; Li, L.; Chen, F.; Zhou, J. Novel Method for Controllable Fabrication of a Superhydrophobic Cuo Surface on Az91d Magnesium Alloy. *ACS Appl Mater Interfaces* **2012**, *4*, 4348-4356.

43. Su, F.; Yao, K. Facile Fabrication of Superhydrophobic Surface with Excellent Mechanical Abrasion and Corrosion Resistance on Copper Substrate by a Novel Method. *ACS Appl Mater Interfaces* **2014**, *6*, 8762-8770.

44. Yuan, S.; Pehkonen, S. O.; Liang, B.; Ting, Y. P.; Neoh, K. G.; Kang, E. T. Superhydrophobic Fluoropolymer-Modified Copper Surface Via Surface Graft Polymerisation for Corrosion Protection. *Corros. Sci.* **2011**, *53*, 2738-2747.

45. Yuan, S.; Xu, F.; Kang, E.; Pehkonen, S. Modification of Surface-Oxidized Copper Alloy by Coupling of Viologens for Inhibiting Microbiologically Influenced Corrosion. *J. Electrochem. Soc.* **2007**, *154*, C645-C657.

46. Boinovich, L. B.; Emelyanenko, A. M. The Behaviour of Fluoro- and Hydrocarbon Surfactants Used for Fabrication of Superhydrophobic Coatings at Solid/Water Interface. *Colloids Surf., A* **2015**, *481*, 167-175.

47. Shen, L.; Qiu, W.; Wang, W.; Xiao, G.; Guo, Q. Facile Fabrication of Superhydrophobic Conductive Graphite Nanoplatelet/Vapor-Grown Carbon Fiber/Polypropylene Composite Coatings. *Compos. Sci. Technol.* **2015**, *117*, 39-45.

48. Wang, Y.; Zhang, H.; Liu, X.; Zhou, Z. Slippery Liquid-Infused Substrates: A Versatile Preparation, Unique Anti-Wetting and Drag-Reduction Effect on Water. *J. Mater. Chem. A* **2016**, *4*, 2524-2529.

49. Wong, T. S.; Kang, S. H.; Tang, S. K.; Smythe, E. J.; Hatton, B. D.; Grinthal, A.; Aizenberg, J. Bioinspired Self-Repairing Slippery Surfaces with Pressure-Stable Omniphobicity. *Nature* **2011**, *477*, 443-447.

50. Marmur, A. Wetting on Hydrophobic Rough Surfaces: To Be Heterogeneous or Not to Be? *Langmuir* **2003**, *19*, 8343-8348.

51. Zarzycki, J.; Prassas, M.; Phalippou, J. Synthesis of Glasses from Gels: The Problem of Monolithic Gels. *J. Mater. Sci.* **1982**, *17*, 3371-3379.

52. Chandra, D.; Yang, S.; Soshinsky, A. A.; Gambogi, R. J. Biomimetic Ultrathin Whitening by Capillary-Force-Induced Random Clustering of Hydrogel Micropillar Arrays. *ACS Appl. Mater. Interfaces* **2009**, *1*, 1698-1704.

53. Chakrapani, N.; Wei, B.; Carrillo, A.; Ajayan, P. M.; Kane, R. S. Capillarity-Driven Assembly of Two-Dimensional Cellular Carbon Nanotube Foams. *Proc. Natl. Acad. Sci. U. S. A.* **2004**, *101*, 4009-4012.

54. Dong, S.; Wang, Z.; Wang, Y.; Liu, H. An Experimental Investigation of Enhancement Surface Quality of Micro-Holes for Be-Cu Alloys Using Micro-Edm with Multi-Diameter Electrode and Different Dielectrics. *Procedia CIRP* **2016**, *42*, 257-262.

55. Domke, J.; Radmacher, M. Measuring the Elastic Properties of Thin Polymer Films with the Atomic Force Microscope. *Langmuir* **1998**, *14*, 3320-3325.

56. Meiron, T. S.; Marmur, A.; Saguy, I. S. Contact Angle Measurement on Rough Surfaces. *J. Colloid Interface Sci.* **2004**, *274*, 637-644.

57. Stalder, A. F.; Melchior, T.; Müller, M.; Sage, D.; Blu, T.; Unser, M. Low-Bond Axisymmetric Drop Shape Analysis for Surface Tension and Contact Angle Measurements of Sessile Drops. *Colloids Surf., A* **2010**, *364*, 72-81.

1

2

3

4

5

Figure Captions

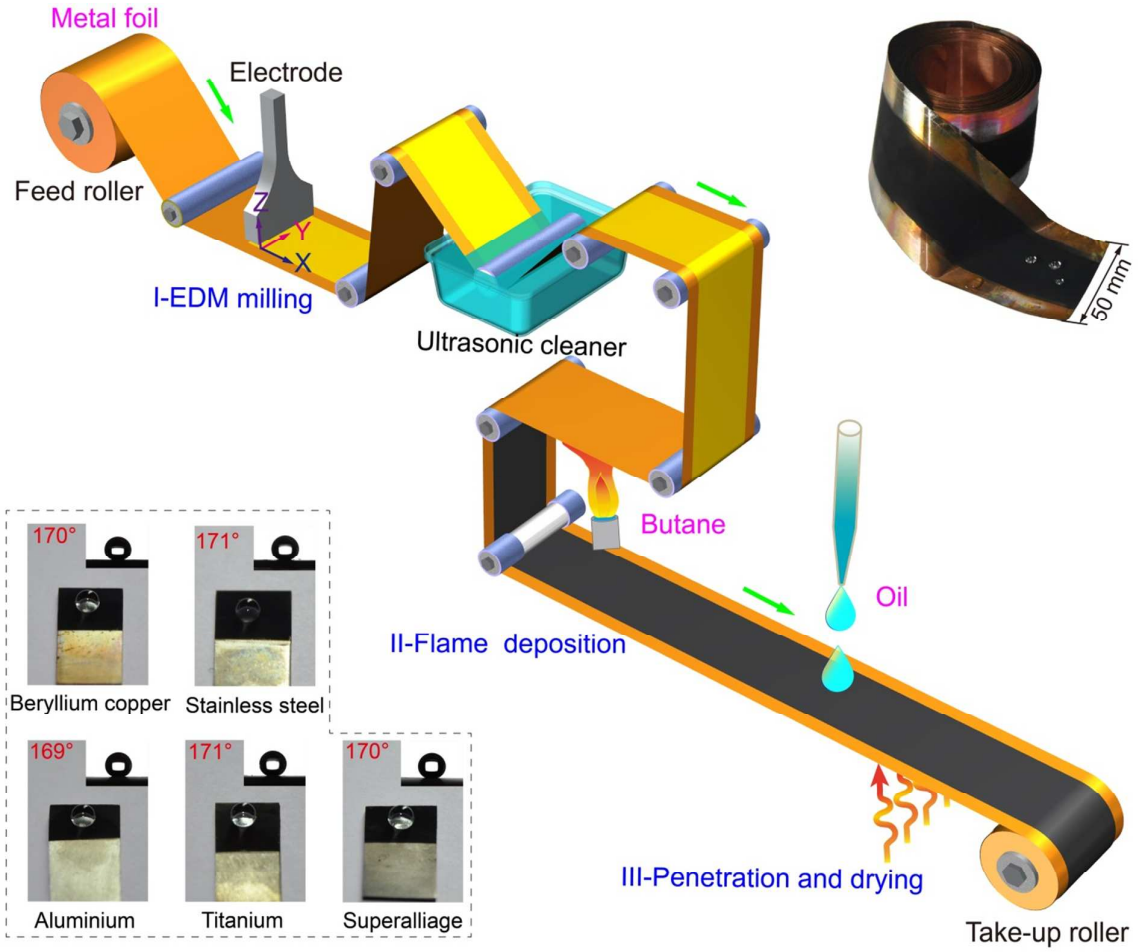

Figure 1. Schematic illustration of roll–to–roll strategy for manufacturing superhydrophobic coating on conventional engineering materials. Step I: Work-piece is milled by EDM process and craters are generated simultaneously. Step II: Milled surface is coated with a layer of soot by the flame of butane. Step III: kerosene penetration and drying the coatings. Inset in bottom left shows superhydrophobic coating on five types of engineering materials with CAs. Inset in top right shows a coils of superhydrophobic coated copper foil (i.e., C17200 beryllium copper alloy).

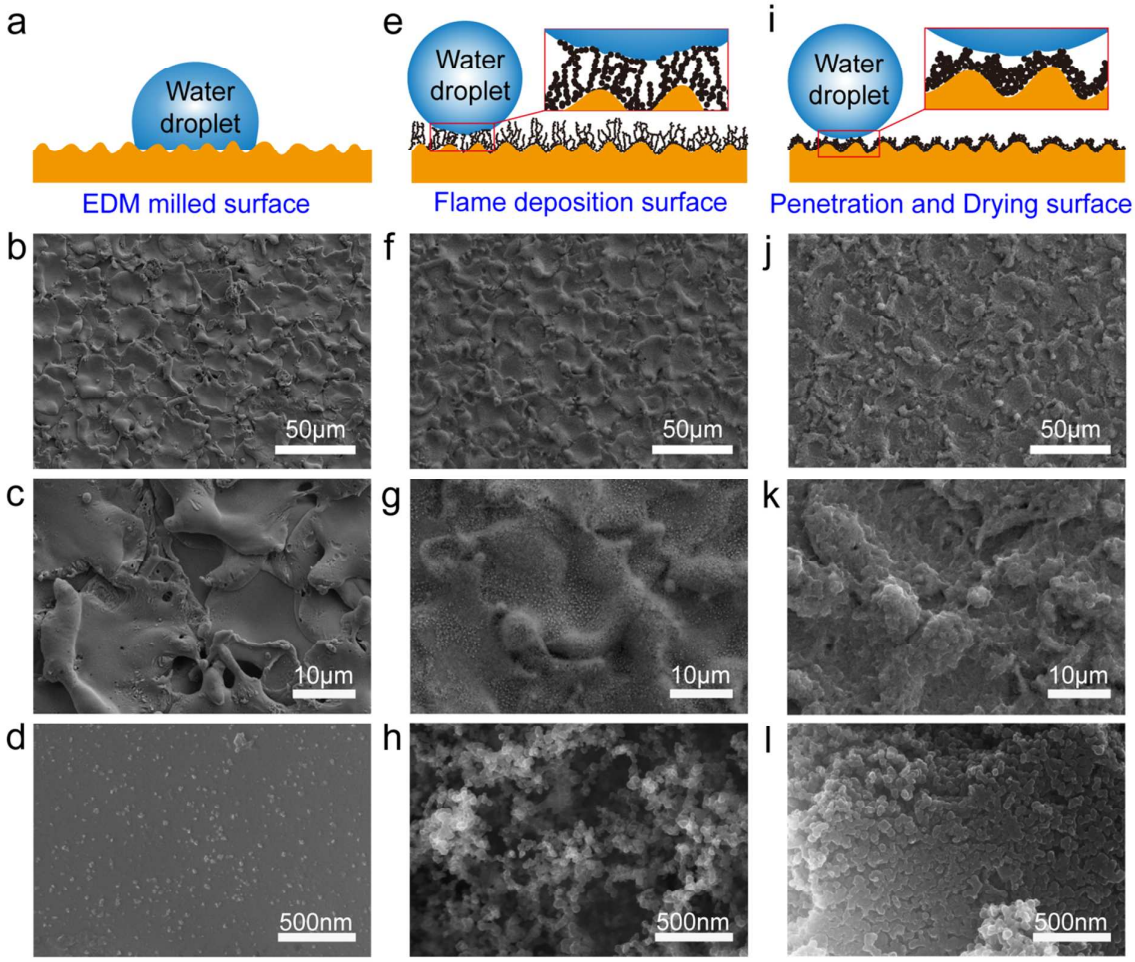

Figure 2. Morphologies evolution of the coating on C17200. (a), (e) and (i) Scheme of morphology of the surface of work-piece during superhydrophobic coating. SEM images of surface morphologies at different magnifications of after EDM milling (b)-(d), flame deposition (f)-(h) and penetration and drying (j)-(l) process.

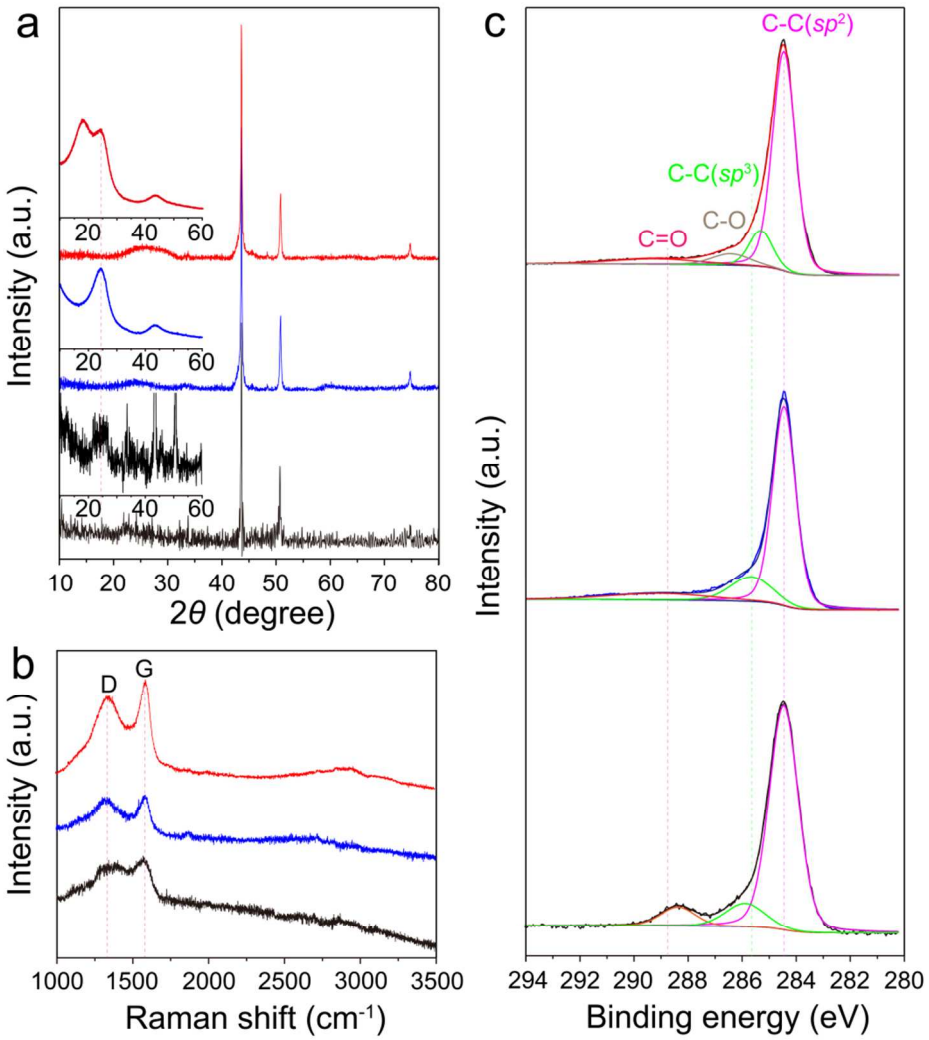

Figure 3. Characterization of chemical structure of superhydrophobic coatings. (a) XRD pattern, (b) Raman spectra and (c) High-resolution XPS scanning of C1s spectra of species after EDM milling (black curve), flame deposition (blue curve) and kerosene penetration drying (red curve), respectively.

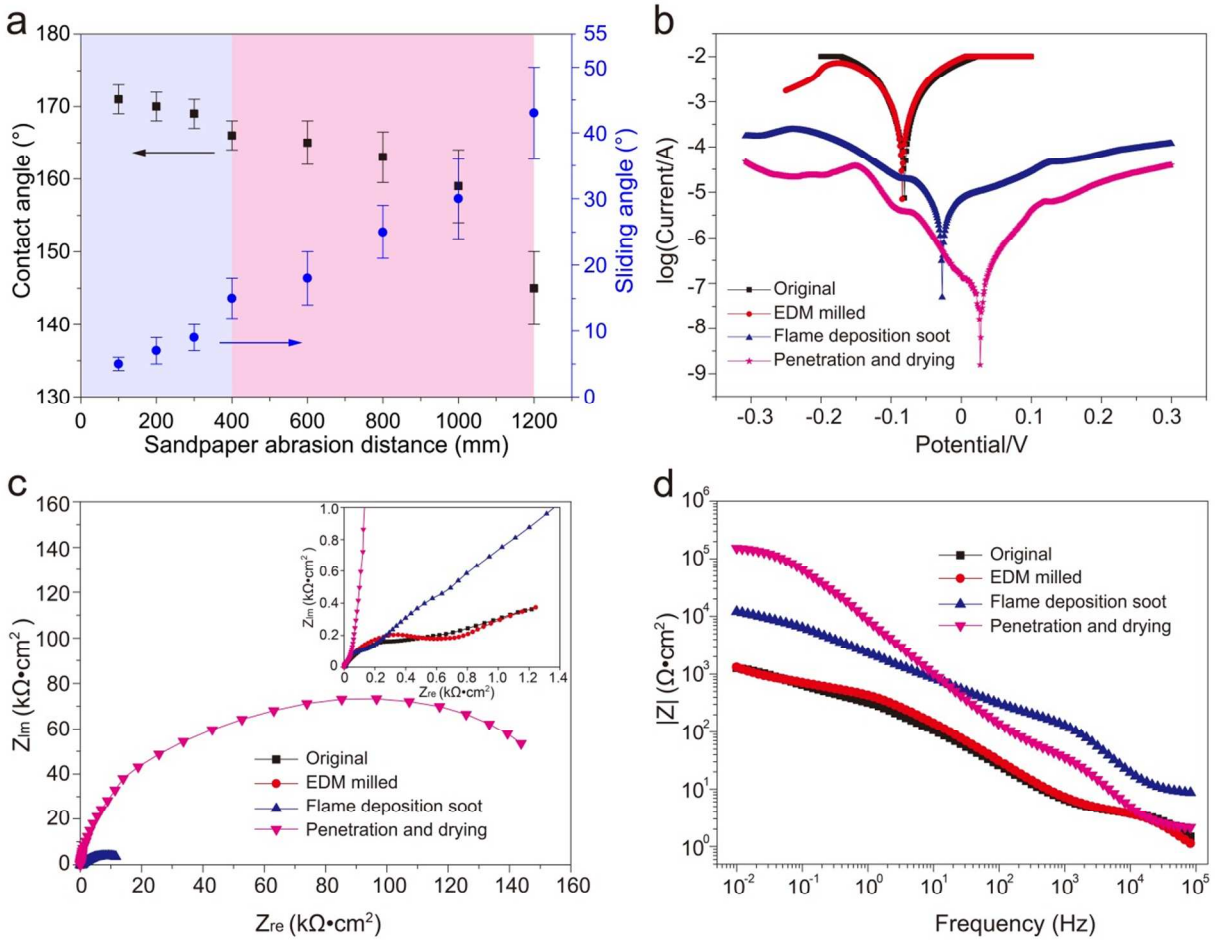

Figure 4. Durability of the superhydrophobic coatings. (a) Plot of mechanical abrasion distance and water contact and sliding angle. (b) Potentiodynamic polarization curves, (c) Nyquist plots and (d) Bode plots of the original beryllium copper alloy (C17200) surface, EDM milled surface, flame deposition soot and oil penetration and drying surface in the neutral solution (3.5 wt% NaCl) for 30 min. The insets figure in (c) is the enlarged scope of Nyquist plots in the high frequency range.

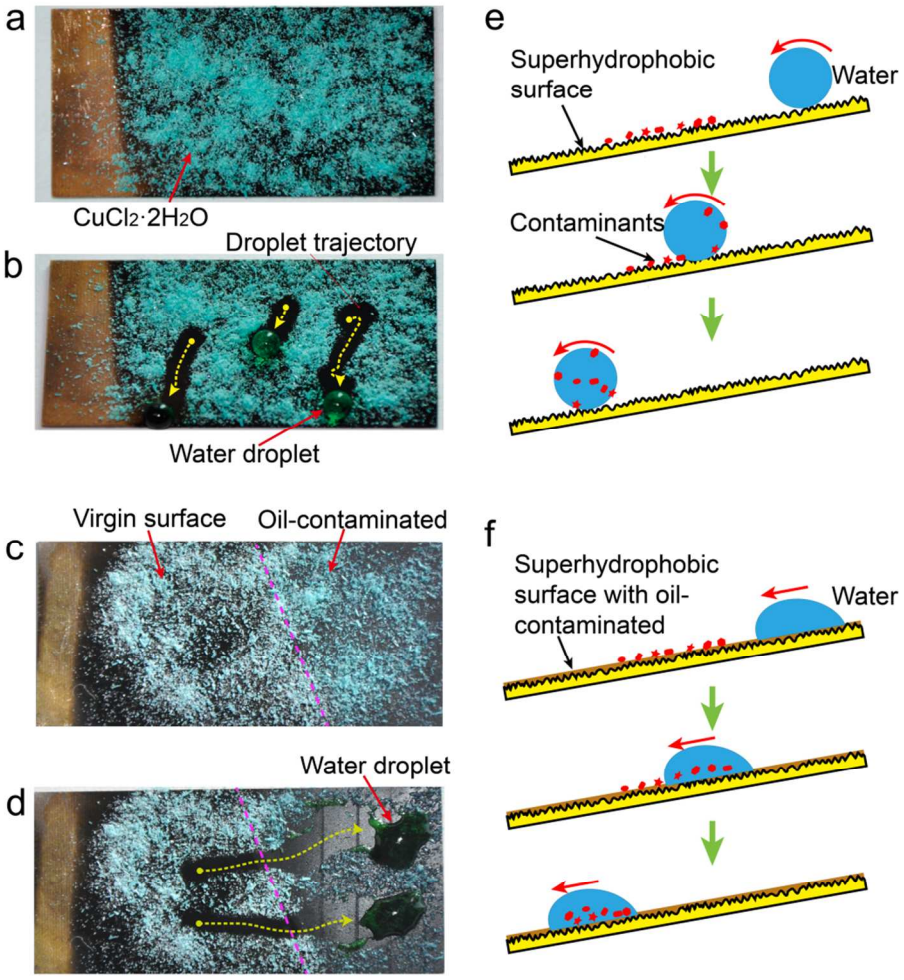

Figure 5. Self-cleaning performance of superhydrophobic coating on C17200. (a) Artificial dirt ($CuCl_2 \cdot 2H_2O$) spread on coating surface. (b) Water droplets roll off on coating surface with dirt. (c) Artificial dirt ($CuCl_2 \cdot 2H_2O$) spread on coating surface pre- contaminated by oil. (d) Water droplets roll off on coating surface after oil contaminated. (e), (f) Mechanism of self-cleaning processs of as-developed superhydrophobic coating and after oil contaminated, respectively.

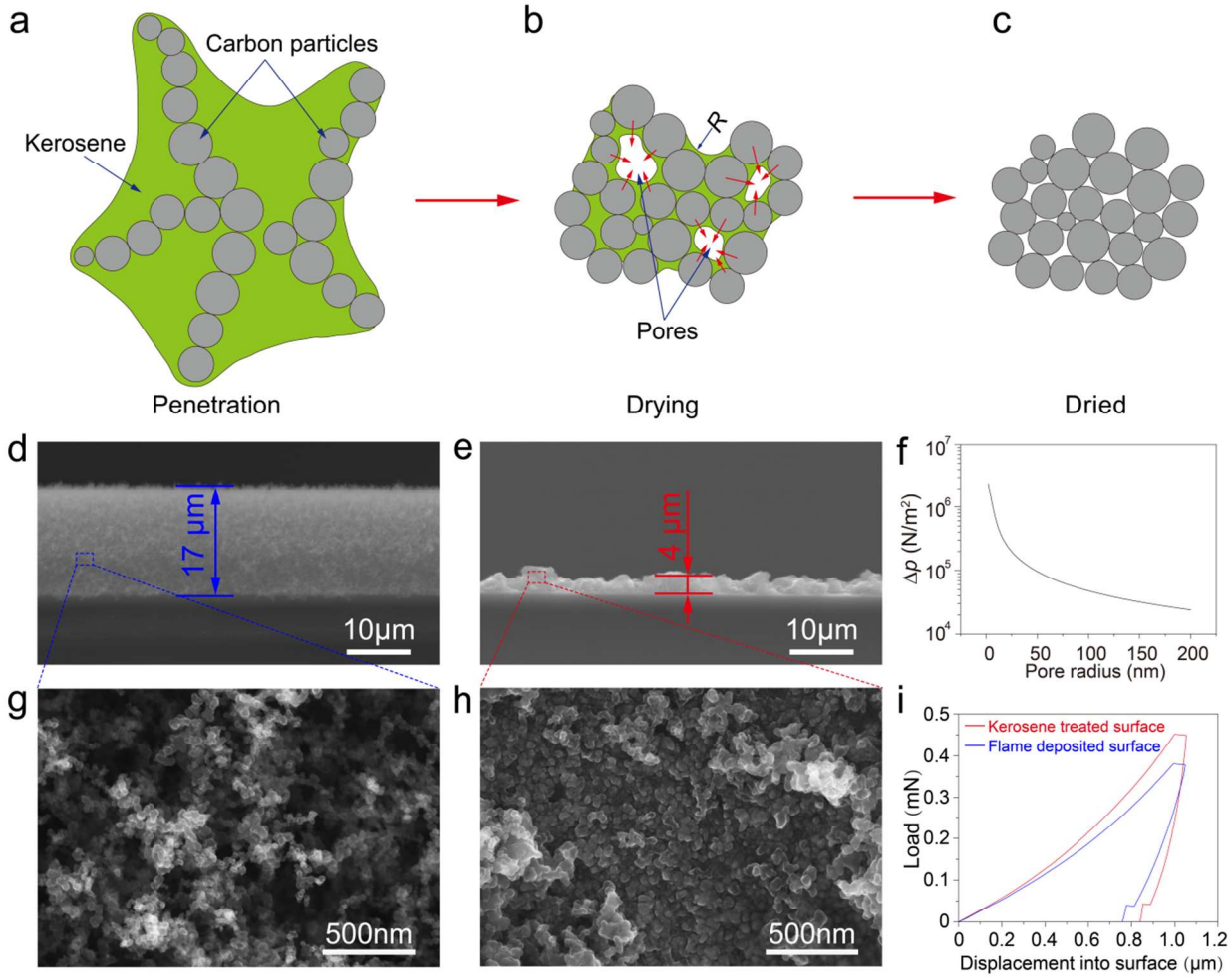

Figure 6. Enhancement of durability of superhydrophobic coatings after kerosene penetration and drying process. (a)-(c) Schematic illustration of penetration and drying process of flame deposited carbon nanoparticles film with kerosene. (d), (e) Cross–section SEM images of flame deposition carbon soot and after kerosense penetration and drying. (f) Capillary pressure (Δp) as a function of pore radius. (g), (h) Enlarged SEM images of (d) and (e) show morphology of carbon soot. (i) Load–displacement curve as the flame deposition film and after kerosene penetration and drying taken from nanoindentation.

Roll–to–Roll Manufacturing of Robust Superhydrophobic Coating on Metallic Engineering Materials

TOC

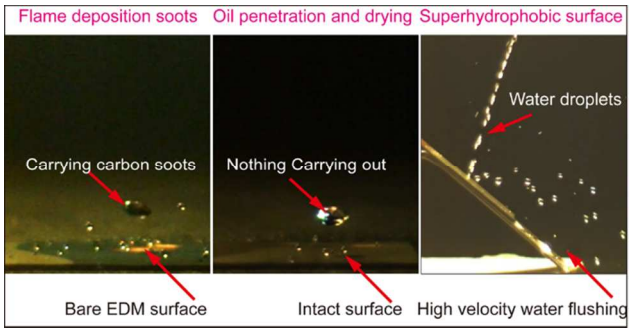

For table of content only